ATLAS NOTE

ATLAS-CONF-2013-097

September 13, 2013

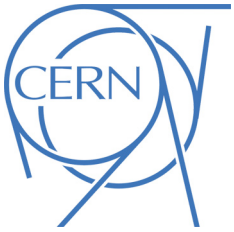

Measurement of the $t\bar{t}$ production cross-section in pp collisions at $\sqrt{s} = 8$ TeV using $e\mu$ events with b-tagged jets

The ATLAS Collaboration

Abstract

This note describes a measurement of the inclusive top-pair production cross-section ($\sigma_{t\bar{t}}$) with the full 2012 ATLAS data sample of 20.3 fb^{-1} of proton-proton collision data at a centre-of-mass energy of $\sqrt{s} = 8$ TeV, using $t\bar{t}$ events with an opposite-sign $e\mu$ pair in the final state. Jets containing b quarks were tagged using an algorithm based on track impact parameters and reconstructed secondary vertices. The numbers of events with exactly one and exactly two b-tagged jets were counted and used to simultaneously determine $\sigma_{t\bar{t}}$ and the efficiency to reconstruct and b-tag a jet from a top quark decay, thereby minimising the associated systematic uncertainties. The cross-section was measured to be:

$$\sigma_{t\bar{t}} = 237.7 \pm 1.7\,(\text{stat}) \pm 7.4\,(\text{syst}) \pm 7.4\,(\text{lumi}) \pm 4.0\,(\text{beam energy})\ \text{pb},$$

where the four uncertainties arise from data statistics, experimental and theoretical systematic effects, the integrated luminosity, and the LHC beam energy, giving a total relative uncertainty of 4.8 %. The result is consistent with recent theoretical QCD calculations at next-to-next-to-leading order.

ATLAS-CONF-2013-097
15 September 2013

1 Introduction

The top quark is the heaviest known fundamental particle, with a mass (m_{top}) that is much larger than any of the other quarks, and close to the scale of electroweak symmetry breaking. The study of its production and decay properties forms a core part of the ATLAS physics programme at the CERN Large Hadron Collider (LHC). At the LHC, top quarks are primarily produced in quark-antiquark pairs ($t\bar{t}$), and the precise prediction of the corresponding inclusive cross-section ($\sigma_{t\bar{t}}$) is a substantial challenge for QCD calculational techniques, as well as being sensitive to the gluon parton density function (PDF), the top quark mass, and potential enhancements due to physics beyond the Standard Model.

Calculations of $\sigma_{t\bar{t}}$ at hadron colliders are now available at full next-to-next-to-leading order (NNLO) accuracy, including the resummation of next-to-next-to-leading logarithmic (NNLL) soft gluon terms [1]. At a centre-of-mass energy of $\sqrt{s} = 8\,\text{TeV}$ and assuming $m_{\text{top}} = 172.5\,\text{GeV}$, these calculations give a prediction of $252.9 \pm 11.7\,^{+6.4}_{-8.6}\,\text{pb}$, where the first uncertainty is due to PDF and α_s uncertainties, and the second to QCD scale uncertainties. This value has been calculated using the `top++ 2.0` program [2]. The PDF and α_s uncertainties were calculated using the PDF4LHC prescription [3] with the MSTW2008 68 % CL NNLO [4], CT10 NNLO [5, 6] and NNPDF2.3 5f FFN [7] PDF sets, and added in quadrature to the scale uncertainty to give a final value of $252.9^{+13.3}_{-14.5}\,\text{pb}$. The NNLO+NNLL cross-section value is about 3 % larger than the exact NNLO prediction, as implemented in `Hathor` 1.5 [8].

Within the Standard Model, the top quark decays almost exclusively to a W boson and a b quark, so the final-state topologies in $t\bar{t}$ production are governed by the decay modes of the two W bosons. This document describes a measurement in the dileptonic $e\mu$ channel, $t\bar{t} \to WbWb \to e^+\mu^-\nu\bar{\nu}b\bar{b}$, selecting events with an opposite-sign $e\mu$ pair,[1] and one or two hadronic jets from the b quarks. Jets originating from b quarks were identified ('tagged') using a b-tagging algorithm exploiting the long lifetime, high decay multiplicity, hard fragmentation and high mass of B hadrons. The rates of events with an $e\mu$ pair and one or two tagged b-jets were used to measure simultaneously the $t\bar{t}$ production cross-section and the combined probability to reconstruct and b-tag a b-jet from a top-quark decay. Events with electrons or muons produced via leptonically decaying taus, $t \to Wb \to \tau\nu b \to e/\mu\nu\nu\nu b$, were included as part of the $t\bar{t}$ signal. The main background is Wt, the associated production of a W boson and a single top quark. Other background contributions arise from $Z \to \tau\tau \to e\mu$+jets production, diboson+jets production and events where one reconstructed lepton does not arise from a W or Z decay.

The data and Monte Carlo simulation samples are described in Section 2, followed by the object and event selection in Section 3, and the extraction of the $t\bar{t}$ cross-section in Section 4. Systematic uncertainties are discussed in Section 5, followed by additional studies and checks in Section 6, and a summary and conclusion are given in Section 7.

2 Data and simulation samples

The ATLAS detector [9] at the LHC covers nearly the entire solid angle around the collision point, and consists of an inner tracking detector surrounded by a thin superconducting solenoid magnet producing a 2 T axial magnetic field, electromagnetic and hadronic calorimeters, and an external muon spectrometer incorporating three large toroid magnet assemblies. The inner detector consists of a high-granularity silicon pixel detector and a silicon microstrip tracker, together providing precision tracking in the range $|\eta| < 2.5$, [2] complemented by a transition radiation tracker providing tracking and electron identification

[1] Charge-conjugate modes are implied throughout.

[2] ATLAS uses a right-handed coordinate system with its origin at the nominal interaction point in the centre of the detector, and the z axis along the beam line. Pseudorapidity is defined in terms of the polar angle θ as $\eta = -\ln\tan\theta/2$, and transverse momentum and energy are defined relative to the beamline as $p_{\text{T}} = p\sin\theta$ and $E_{\text{T}} = E\sin\theta$. The azimuthal angle around the beam line is denoted by ϕ, and distances in (η, ϕ) space by $\Delta R = \sqrt{\Delta\eta^2 + \Delta\phi^2}$.

information for $|\eta| < 2.0$. A lead liquid-argon (LAr) electromagnetic calorimeter covers the region $|\eta| < 3.2$, and hadronic calorimetry is provided by steel/scintillating tile calorimeters for $|\eta| < 1.7$ and copper/LAr hadronic endcap calorimeters. The forward region is covered by additional LAr calorimeters with copper and tungsten absorbers. The muon spectrometer consists of precision tracking chambers covering the region $|\eta| < 2.7$, and separate trigger chambers covering $|\eta| < 2.4$. A three-level trigger system, using custom hardware followed by two software-based levels, is used to reduce the event rate to about 400 Hz for offline storage.

The analysis was performed on the complete ATLAS 2012 $\sqrt{s} = 8$ TeV proton-proton collision data sample, corresponding to an integrated luminosity of 20.3 fb^{-1} after the application of detector status and data quality requirements. Events were required to pass either a single electron or single muon trigger, with thresholds set to be fully efficient for leptons with $p_{\mathrm{T}} > 25$ GeV passing offline selections. Due to the high instantaneous luminosities achieved by the LHC in 2012, each triggered event also includes the signals from typically 10–30 additional inelastic pp collisions in the same bunch crossing (pileup).

Monte Carlo simulated event samples were used to develop the analysis, to compare to the data and to evaluate signal and background efficiencies and uncertainties. Samples were processed either through the full ATLAS detector simulation [10] based on GEANT4 [11], or through a faster simulation making use of parameterised showers in the calorimeters [12]. Additional simulated pp collisions generated with Pythia 8 [13] were overlaid to simulate the effects of both in- and out-of-time pileup, from additional pp collisions in the same and nearby bunch crossings. All simulated events were then processed using the same reconstruction algorithms and analysis chain as the data, and small corrections were applied to lepton trigger and reconstruction efficiencies to better model the response seen in data.

The baseline $t\bar{t}$ full simulation sample was produced using the next-to-leading-order (NLO) matrix element generator Powheg [14] interfaced to Pythia6 [15] with the Perugia 2011C tune (P2011C) [16], and CT10 PDFs [5], including all $t\bar{t}$ final states involving at least one lepton. The Standard Model expectation of 0.1082 was assumed for the $W \to \ell\nu$ branching ratio [17], and m_{top} was set to 172.5 GeV. Alternative $t\bar{t}$ samples were produced with MC@NLO [18] interfaced to Herwig [19] with Jimmy [20] for the underlying event modelling, with the ATLAS AUET2 [21] tune and CT10 PDFs, and with the leading-order multileg generatorAlpgen [22] interfaced to Herwig and Jimmy, with the CTEQ6L1 PDFs [23] and including $t\bar{t}$ final states with up to three additional partons.

Backgrounds were classified into two types: those with two real prompt leptons from W or Z decays (including those produced via leptonic tau decays), and those where at least one of the reconstructed lepton candidates is misidentified or 'fake', *i.e.* a non-prompt lepton from the decay of a bottom or charm hadron, an electron from a photon conversion in a jet, hadronic jet activity misidentified as an electron, or a muon produced from an in-flight decay of a pion or kaon. The first category with two prompt leptons includes Wt single top production, modelled using Powheg+Pythia6 with the CT10 PDFs and the P2011C tune, $Z \to \tau\tau$+jets modelled using Alpgen+Pythia6 with CTEQ6L1 PDFs and P2011C, and diboson (WW, WZ, ZZ) production in association with jets, modelled using Alpgen+Herwig. Backgrounds with one real and one fake lepton include $t\bar{t}$ events where one W boson decays hadronically, W+jets production, modelled as for Z+jets, and t-channel single top production, modelled using AcerMC [24] interfaced to Pythia6 with CTEQ6L1 PDFs. Other backgrounds, including processes with two fake leptons, are negligible for the event selections used in this analysis.

3 Object and event selection

This analysis makes use of reconstructed electrons, muons and b-tagged jets. Electron candidates were reconstructed from an isolated electromagnetic calorimeter energy deposit matched to an inner detector track and passing tight identification requirements [25], with transverse energy $E_{\mathrm{T}} > 25$ GeV and pseudorapidity $|\eta| < 2.47$. Candidates within the transition region between the barrel and endcap elec-

tromagnetic calorimeters, $1.37 < |\eta| < 1.52$, were removed. Isolation requirements were used to reduce background from non-prompt electrons. The calorimeter transverse energy within a cone of $\Delta R < 0.2$ and the scalar sum of track p_{T} within $\Delta R < 0.3$ were each required to be smaller than E_{T} and η-dependent thresholds calibrated to separately give nominal selection efficiencies of 98 % for prompt electrons from $Z \to ee$ decays.

Muon candidates were reconstructed by combining matching tracks reconstructed in both the inner detector and muon spectrometer, and required to satisfy $p_{\mathrm{T}} > 25\,\mathrm{GeV}$ and $|\eta| < 2.5$. They were also required to satisfy the isolation requirement $I < 0.05$, where I is the ratio of the sum of track p_{T} in a variable-sized cone of radius $\Delta R = 10\,\mathrm{GeV}/p_{\mathrm{T}}^{\mu}$ to the transverse momentum p_{T}^{μ} of the muon [26]. This isolation requirement has a 97 % selection efficiency for prompt muons from $Z \to \mu\mu$ decays.

Jets were reconstructed using the anti-k_t algorithm [27] with radius parameter $R = 0.4$, starting from calorimeter energy clusters calibrated using the local cluster weighting method [28], and corrected for the effects of pileup as described in Ref. [29]. Jets were calibrated using an energy- and η-dependent simulation-based calibration scheme, with in-situ corrections based on data [30], and required to satisfy $p_{\mathrm{T}} > 25\,\mathrm{GeV}$ and $|\eta| < 2.5$. To suppress the contribution from low-p_{T} jets originating from pileup interactions, the jet vertex fraction requirement described in Ref. [29] was applied: jets with $p_{\mathrm{T}} < 50\,\mathrm{GeV}$ and $|\eta| < 2.4$ were required to have at least half of the scalar sum of p_{T} of tracks associated to the jet coming from tracks associated to the event primary vertex. The latter was defined as the reconstructed vertex with the highest sum of associated track p_{T}^2. Finally, to remove non-isolated leptons likely to have come from heavy-flavour decays inside jets, electrons and muons within $\Delta R < 0.4$ of selected jets were also discarded.

Jets were b-tagged as likely to have originated from b quarks using the MV1 algorithm, a multivariate discriminant making use of track impact parameters and reconstructed secondary vertices [31, 32]. Jets were defined to be b-tagged if the MV1 discriminant value was larger than a threshold corresponding approximately to a 70 % efficiency for tagging b-quark jets from top decays in $t\bar{t}$ events, with a rejection factor of about 140 against light quark and gluon jets, and about five against jets originating from charm quarks.

Events were required to have at least one reconstructed primary vertex with at least five associated tracks, and no jets failing jet quality and timing requirements. Events with muons compatible with cosmic ray interactions and muons undergoing catastrophic bremsstrahlung in the detector material were also removed. A preselection requiring exactly one electron and one muon selected as described above was then applied, with at least one of the leptons being matched to an electron or muon object triggering the event. Events with an opposite-sign $e\mu$ pair constituted the main analysis sample, whilst events with a same-sign $e\mu$ pair were used in the estimation of the background from misidentified leptons.

4 Extraction of the $t\bar{t}$ cross-section

The $t\bar{t}$ production cross-section $\sigma_{t\bar{t}}$ was determined by counting the numbers of opposite-sign $e\mu$ events with exactly one (N_1) and exactly two (N_2) b-tagged jets, ignoring any untagged jets which may be present, due *e.g.* to light-quark or gluon jets from QCD radiation or b-jets from top decays which were not tagged. The two event counts can be expressed as:

$$\begin{aligned} N_1 &= L\sigma_{t\bar{t}}\,\epsilon_{e\mu} 2\epsilon_b(1 - C_b\epsilon_b) + N_1^{\mathrm{bkg}} \\ N_2 &= L\sigma_{t\bar{t}}\,\epsilon_{e\mu} C_b {\epsilon_b}^2 + N_2^{\mathrm{bkg}} \end{aligned} \tag{1}$$

where L is the integrated luminosity of the sample and $\epsilon_{e\mu}$ the efficiency for a $t\bar{t}$ event to pass the opposite-sign $e\mu$ preselection. The combined probability for a jet from the quark q in the $t \to Wq$ decay to fall within the acceptance of the detector, be reconstructed as a jet with transverse momentum above the

Event counts	N_1	N_2
Data	21559	11682
Wt single top	2070 ± 220	360 ± 120
Dibosons	120 ± 90	3^{+6}_{-3}
$Z(\rightarrow \tau\tau \rightarrow e\mu)$+jets	210 ± 10	8 ± 1
Misidentified leptons	240 ± 70	110 ± 60
Total background	2640 ± 250	480 ± 140

Table 1: Observed numbers of opposite-sign $e\mu$ events with one and two b-tagged jets (N_1 and N_2), together with the estimates of non-$t\bar{t}$ backgrounds and associated total uncertainties described in Section 5.

selection threshold, and be tagged as a b-jet, is denoted by ϵ_b. Although this quark is almost always a b quark, ϵ_b thus also accounts for the approximately 0.2 % of top quarks that decay to Ws or Wd rather than Wb, slightly reducing the effective tagging efficiency. If the decays of the two top quarks and the subsequent reconstruction of the two b-tagged jets are completely independent, the probability to tag both b-jets ϵ_{bb} is given by $\epsilon_{bb} = {\epsilon_b}^2$. In practice, small correlations are present for both kinematic and instrumental reasons, and these are taken into account via the tagging correlation C_b, defined as $C_b = \epsilon_{bb}/{\epsilon_b}^2$, or equivalently $C_b = 4N_{e\mu}^{t\bar{t}}N_2^{t\bar{t}}/(N_1^{t\bar{t}} + 2N_2^{t\bar{t}})^2$, where $N_{e\mu}^{t\bar{t}}$ is the number of preselected $e\mu$ $t\bar{t}$ events and $N_1^{t\bar{t}}$ and $N_2^{t\bar{t}}$ are the numbers of events with one and two b-tagged jets. This correlation term also accounts for the effect on N_1 and N_2 of the small number of mistagged light quark or gluon jets from radiation in the $t\bar{t}$ events. Background from sources other than $t\bar{t} \rightarrow e\mu\nu\bar{\nu}b\bar{b}$ also contributes to the event counts N_1 and N_2, and is given by the background terms N_1^{bkg} and N_2^{bkg}. The preselection efficiency $\epsilon_{e\mu}$ and tagging correlation C_b were taken from $t\bar{t}$ event simulation, and the background contributions N_1^{bkg} and N_2^{bkg} were estimated using a combination of simulation and data-based methods, allowing the two equations (1) to be solved yielding $\sigma_{t\bar{t}}$ and ϵ_b.

A total of 66119 events passed the $e\mu$ opposite-sign preselection in data. Table 1 shows the number of events with one and two b-tagged jets, together with the estimates of non-$t\bar{t}$ background and their systematic uncertainties discussed in detail below. The sample with one b-tagged jet is expected to be about 89 % pure in $t\bar{t}$ events, with the dominant background coming from Wt single top production, and smaller contributions from events with misidentified leptons, Z+jets and dibosons. The sample with two b-tagged jets is expected to be about 96% pure in $t\bar{t}$ events, with Wt production again being the dominant background.

The distributions of the number of b-tagged jets and the b-tagging weight in opposite-sign $e\mu$ events are shown in Figure 1, and compared to the expectations with several $t\bar{t}$ simulation samples, normalised using the theoretical prediction of 252.9 pb for the $t\bar{t}$ cross-section at $\sqrt{s} = 8$ TeV. Distributions of the number of jets, the jet p_{T}, and the electron and muon $|\eta|$ and p_{T} are shown for opposite-sign $e\mu$ events with at least one b-tagged jet in Figure 2, with the simulation normalised to the same number of events as the data. In general, the agreement between data and simulation is good, within the modelling and instrumental uncertainties of the analysis.

The value of $\sigma_{t\bar{t}}$ extracted from equation (1) is directly sensitive to the assumed value of $\epsilon_{e\mu}$, with $(\mathrm{d}\sigma_{t\bar{t}}/\mathrm{d}\epsilon_{e\mu})/(\sigma_{t\bar{t}}/\epsilon_{e\mu}) = -1$. The value of $\epsilon_{e\mu}$ was determined from simulation to be about 0.8 %, including the $t\bar{t} \rightarrow e\mu\nu\bar{\nu}b\bar{b}$ branching ratio, and uncertainties on $\epsilon_{e\mu}$ translate directly into uncertainties on $\sigma_{t\bar{t}}$. Similarly, $\sigma_{t\bar{t}}$ is directly sensitive to the value of C_b, also determined from simulation, but with the opposite sign, $(\mathrm{d}\sigma_{t\bar{t}}/\mathrm{d}C_b)/(\sigma_{t\bar{t}}/C_b) = 1$. The systematic uncertainties on these quantities are discussed in Section 5.

With the kinematic cuts and b-tagging working point chosen for this analysis, the sensitivities of $\sigma_{t\bar{t}}$ to the knowledge of the backgrounds N_1^{bkg} and N_2^{bkg} are given by $(\mathrm{d}\sigma_{t\bar{t}}/\mathrm{d}N_1^{\text{bkg}})/(\sigma_{t\bar{t}}/N_1^{\text{bkg}}) = -0.13$ and

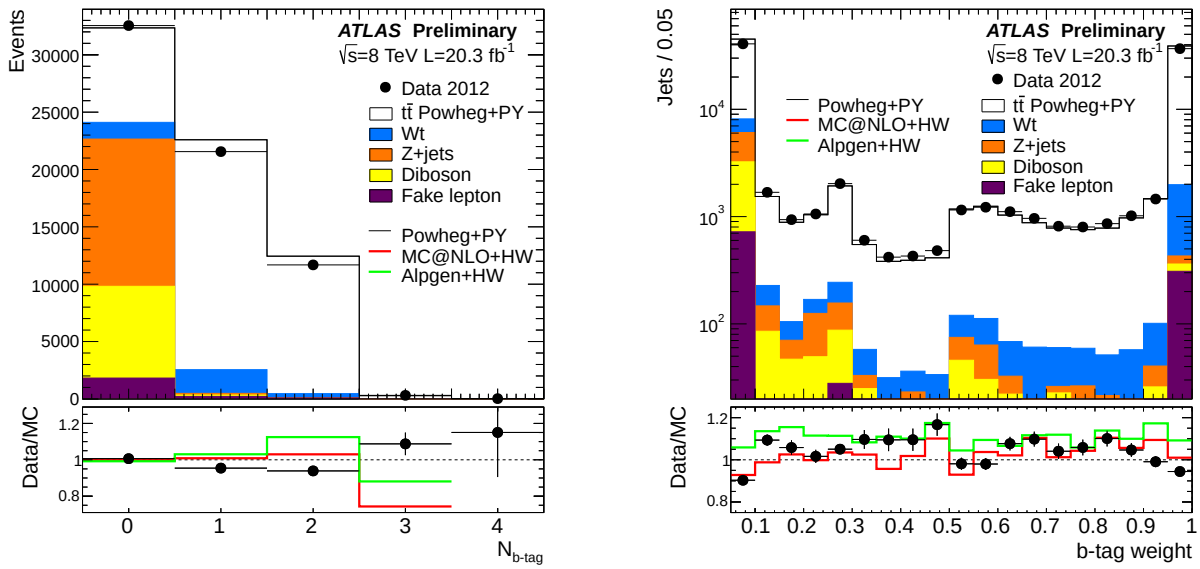

(a) (b)

Figure 1: Distributions of (a) the number of b-tagged jets, and (b) the b-tag weight (also requiring the event to have at least two jets), in preselected opposite-sign $e\mu$ events. The data are shown compared to the expectation from simulation, broken down into contributions from $t\bar{t}$, Wt single top, Z+jets, dibosons, and events with fake electrons or muons, normalised to the same integrated luminosity as the data. The lower parts of the figure show the ratios of data to the baseline prediction using POWHEG+PYTHIA (PY) for the $t\bar{t}$ signal, and the ratios of the predictions with the other $t\bar{t}$ samples using MC@NLO+HERWIG (HW) and ALPGEN+HERWIG to the baseline prediction.

$(\mathrm{d}\sigma_{t\bar{t}}/\mathrm{d}N_2^{\mathrm{bkg}})/(\sigma_{t\bar{t}}/N_2^{\mathrm{bkg}}) = -0.004$. The fitted cross-section is therefore most sensitive to the systematic uncertainties on N_1^{bkg}, whilst for the b-tagging working point chosen for the analysis, the measurement of N_2 serves mainly to constrain the combined jet reconstruction and b-tagging efficiency ϵ_b. As discussed in Section 6, consistent results were also obtained at different b-tagging efficiency working points, that induce greater sensitivity to the background estimate in the two b-tag sample.

The Wt single top background was estimated from simulation using POWHEG+PYTHIA with the P2011C tune, normalised to the approximate NNLO cross-section of 22.37 ± 1.52 pb determined as in Ref. [33]. The diboson background was similarly estimated using ALPGEN+HERWIG, normalised to the NLO QCD inclusive cross-section predictions calculated with MCFM [34].

The Z+jets background (with $Z \to \tau\tau \to e\mu$) was estimated from simulation using ALPGEN+PYTHIA, scaled by the ratios of $Z \to \mu\mu$+jets measured in data and simulation. The ratio was evaluated separately in the one and two b-tag event bins. This scaling eliminates uncertainties due to the simulation modelling of jets (especially heavy-flavour jets) produced in association with the Z bosons. The data/simulation ratios were measured in events with exactly two opposite-sign muons passing the selections given in Section 3 and one or two b-tagged jets, by fitting the dimuon invariant mass distributions in the range 60–120 GeV and accounting for the backgrounds from $t\bar{t}$ production and fake leptons. The resulting scale factors were determined to be 1.43 ± 0.07 and 1.21 ± 0.09 for the one and two b-tag backgrounds, where the systematic uncertainties were derived from a comparison of the $Z \to \mu\mu$ results with those obtained using the same fit technique in $Z \to ee$ events, which have different backgrounds.

The background from events with one real and one fake lepton was estimated using a combination of data and simulation. Simulation studies show that the samples with a same-sign $e\mu$ pair and one

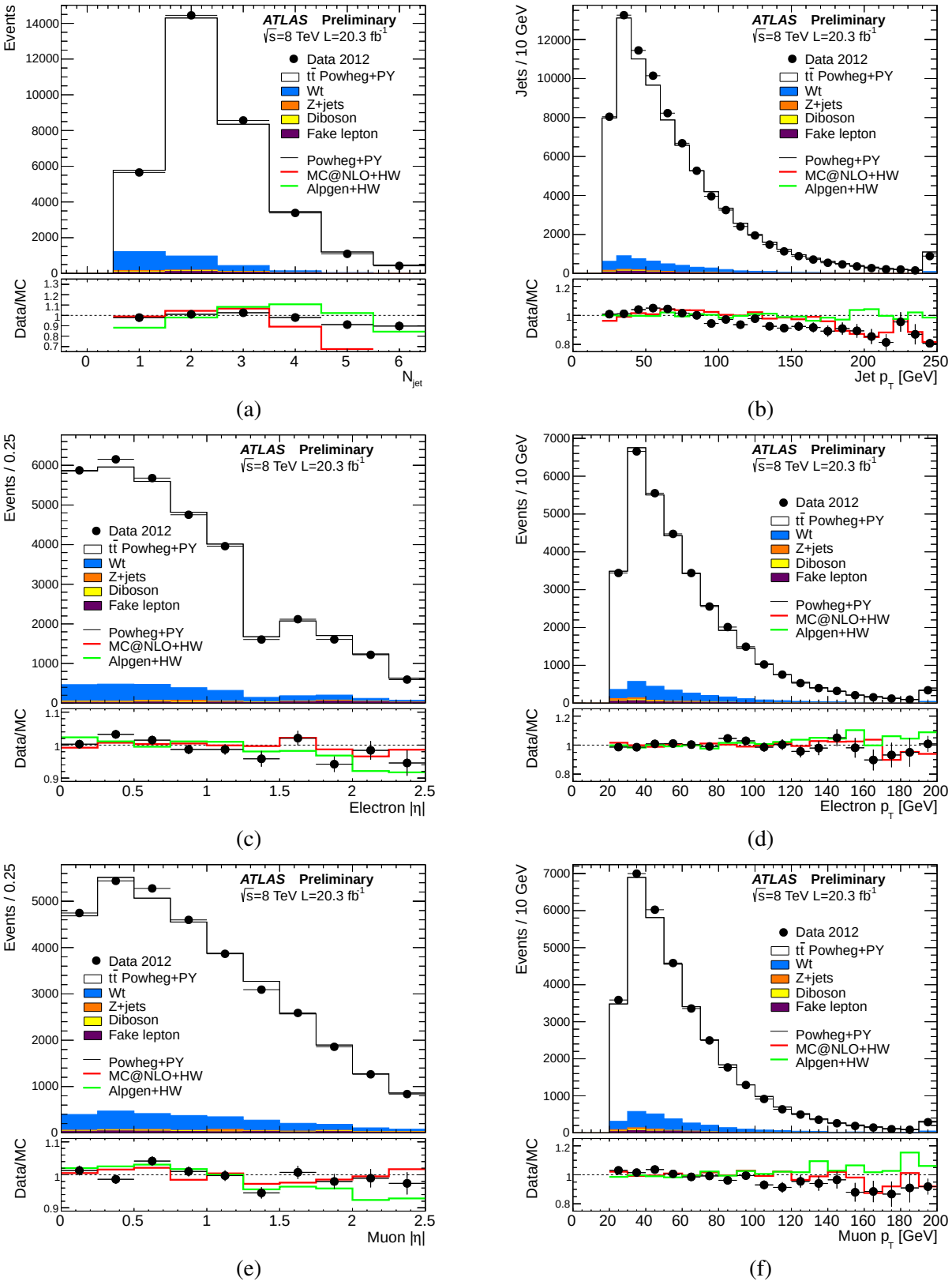

Figure 2: Distributions of (a) the number of jets, (b) the transverse momentum p_{T} of the jets, (c) the $|\eta|$ of the electron, (d) the p_{T} of the electron, (e) the $|\eta|$ of the muon and (f) the p_{T} of the muon, in events with an opposite-sign $e\mu$ pair and at least one b-tagged jet. The data are compared to the expectation from simulation, broken down into contributions from $t\bar{t}$, single top, Z+jets, dibosons, and events with fake electrons or muons, normalised to the same number of entries as the data. The lower parts of the figures show the ratios of data to the baseline prediction with POWHEG+PYTHIA, and the ratios of the predictions with the other $t\bar{t}$ generators to the baseline prediction. The last histogram bin includes the overflow.

Component	OS 1b	SS 1b	(OS/SS) 1b	OS 2b	SS 2b	(OS/SS) 2b
Heavy-flavour e	32 ± 3	24 ± 3	1.35 ± 0.23	5 ± 1	2 ± 1	2.15 ± 0.85
Conversion e	139 ± 9	127 ± 10	1.09 ± 0.11	79 ± 5	55 ± 4	1.43 ± 0.13
Other e	17.4 ± 7.3	0.4 ± 0.3	-	4.8 ± 1.1	0.2 ± 0.2	-
Heavy-flavour μ	25 ± 5	18 ± 3	1.38 ± 0.37	2 ± 1	3 ± 1	0.95 ± 0.45
Other μ	2.3 ± 1.1	0.7 ± 0.4	-	0.8 ± 0.4	0.0 ± 0.0	-
Total fake	215 ± 14	170 ± 11	1.26 ± 0.09	92 ± 5	60 ± 4	1.52 ± 0.09
Wrong-sign prompt	-	32 ± 3	-	-	11 ± 2	-
Right-sign prompt	-	19 ± 2	-	-	0 ± 0	-
Total	-	221 ± 12	-	-	71 ± 4	-
Data	-	240	-	-	83	-

Table 2: Breakdown of expected fake-lepton event contributions to the one (1b) and two (2b) b-tag opposite and same-sign (OS and SS) $e\mu$ event samples, together with the opposite- to same-sign ratios for contributions from heavy flavour and photon conversions, and for all fake lepton categories combined. For the same-sign samples, the contributions from wrong- and right-sign prompt lepton contributions are also shown, and the total expectations are compared to the data. The uncertainties shown are due to limited simulation statistics.

or two b-tagged jets are dominated by events with fake leptons, with rates comparable to those in the opposite-sign sample. The contributions of fake-lepton events were therefore estimated using the same-sign event counts in data after subtraction of the estimated non-fake same-sign contributions, multiplied by the opposite- to same-sign fake-lepton ratios predicted from simulation. This procedure is illustrated in Table 2, which shows the expected numbers of fake-lepton events in opposite- and same-sign samples. The contributions where the electron is fake, coming from the decay of a heavy-flavour hadron, a photon conversion or other sources (such as a misidentified hadron within a jet), and where the muon is fake, coming either from heavy-flavour decay or other sources (e.g. decay in flight of a pion or kaon) are shown separately. In all samples, the dominant fake lepton contribution comes from photon conversions giving electron candidates. The opposite- to same-sign ratios $R_j = N_j^{\text{fake,OS}}/N_j^{\text{fake,SS}}$ for events with $j = 1$ and 2 b-tagged jets were evaluated from simulation to be $R_1 = 1.26$ and $R_2 = 1.52$, with systematic uncertainties of 25 % and 50 %. These uncertainties were derived considering the different R_j values observed in simulation for individual components of the fake-lepton background, and possible variations in the background composition. Table 2 also shows the contributions to the same-sign samples of events with two prompt leptons, divided into 'wrong-sign' events where the charge of the electron has been misreconstructed, dominated by genuine $t\bar{t} \to e\mu\nu\bar{\nu}b\bar{b}$, and 'right-sign' events, dominated by diboson production with two like-sign W bosons. A 50 % uncertainty was conservatively assigned to the prompt lepton contribution, based on studies of the simulation modelling of the electron charge-misidentification probability in data [25] and uncertainties in the rates of contributing physics processes.

The simulation modelling of the different components of the fake-lepton background was checked by studying kinematic distributions of same-sign events, as illustrated for the η and p_{T} distributions of the leptons in Figure 3. The simulation generally models the shapes of distributions well in both one and two b-tag events, and agrees with the overall same-sign rates in data within about 20 %. The simulation modelling was further tested in control samples with relaxed electron or muon isolation requirements to enhance the relative contributions of electrons or muons from heavy-flavour decays, and similar levels of agreement were seen.

Combining the estimates of $\epsilon_{e\mu}$ and C_b from the baseline Powheg+Pythia simulation, the estimates of the background N_1^{bkg} and N_2^{bkg} shown in Table 1 and the data integrated luminosity of 20.3 fb^{-1}, the $t\bar{t}$

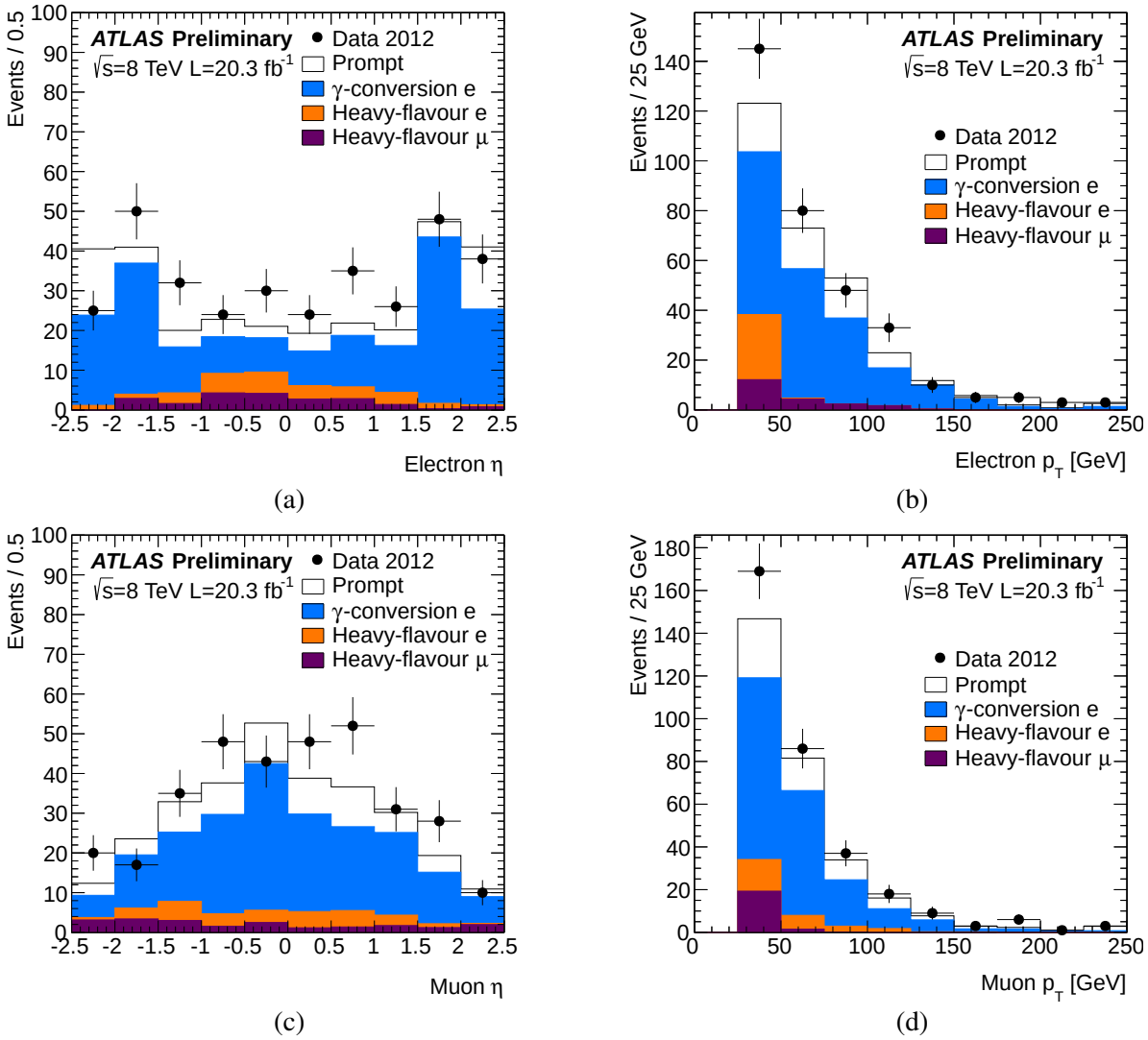

Figure 3: Distributions of electron and muon η and p_{T} in same-sign $e\mu$ events with at least one b-tagged jet. The simulation prediction is normalised to the same integrated luminosity as the data, and broken down into contributions where both leptons are prompt, or one is a fake lepton from a photon conversion or heavy-flavour decay. In the p_{T} distributions, the last histogram bin includes the overflows.

cross-section was determined by solving equation (1) numerically to be:

$$\sigma_{t\bar{t}} = 237.7 \pm 1.7\,\mathrm{pb},$$

where the uncertainty quoted is due to data statistics only. The product of jet reconstruction and b-tagging efficiencies ϵ_b was measured to be 0.540 ± 0.003, compared to 0.543 ± 0.001 in simulation.

5 Systematic uncertainties

The systematic uncertainties on the extracted cross-section $\sigma_{t\bar{t}}$ and ϵ_b are shown in Table 3, together with their effects (where relevant) on the $t\bar{t}$ preselection efficiency $\epsilon_{e\mu}$ and tagging correlation C_b. Each source of uncertainty was evaluated by repeating the fit with all relevant input parameters simultaneously changed by ± 1 standard deviation. Systematic correlations between input parameters (in particular

Uncertainty	$\Delta\epsilon_{e\mu}/\epsilon_{e\mu}$ (%)	$\Delta C_b/C_b$ (%)	$\Delta\sigma_{t\bar{t}}/\sigma_{t\bar{t}}$ (%)	$\Delta\sigma_{t\bar{t}}$ (pb)	$\Delta\epsilon_b/\epsilon_b$ (%)
Data statistics	-	-	0.72	1.7	0.57
$t\bar{t}$ modelling	0.91	-0.61	1.52	3.6	0.61
Initial/final state radiation	-0.76	0.26	1.23	2.9	0.37
Parton density functions	1.08	-	1.09	2.6	0.06
QCD scale choices	0.30	-	0.30	0.7	0.00
Single-top modelling	-	-	0.38	0.9	0.56
Single-top/$t\bar{t}$ interference	-	-	0.15	0.4	0.25
Single-top Wt cross-section	-	-	0.70	1.7	0.24
Diboson modelling	-	-	0.42	1.0	0.19
Diboson cross-sections	-	-	0.03	0.1	0.01
Z+jets extrapolation	-	-	0.05	0.1	0.02
Electron energy scale/resolution	0.43	0.01	0.48	1.1	0.03
Electron identification/isolation	1.28	0.00	1.42	3.4	0.05
Muon momentum scale/resolution	0.01	0.01	0.05	0.1	0.02
Muon identification/isolation	0.50	0.00	0.52	1.2	0.01
Lepton trigger	0.15	0.00	0.16	0.4	0.01
Jet energy scale	0.46	0.07	0.49	1.2	0.11
Jet energy resolution	-0.44	0.04	0.59	1.4	0.08
Jet reconstruction/vertex fraction	0.02	0.01	0.04	0.1	0.01
b-tagging	-	0.13	0.42	1.0	0.09
Pileup modelling	-0.30	0.05	0.28	0.7	0.05
Misidentified leptons	-	-	0.38	0.9	0.12
Total systematic	2.29	0.69	3.12	7.4	1.02
Integrated luminosity	-	-	3.11	7.4	0.11
LHC beam energy	-	-	1.70	4.0	0.00
Total uncertainty	2.29	0.69	4.77	11.3	1.17

Table 3: Summary of the statistical, systematic and total uncertainties on the $t\bar{t}$ production cross-section $\sigma_{t\bar{t}}$ and the combined jet reconstruction and b-tagging efficiency ϵ_b. The systematic uncertainties on the $e\mu$ preselection efficiency $\epsilon_{e\mu}$ and the tagging correlation C_b are also shown, with relative signs given where relevant. The sign definitions are given in the text.

significant anti-correlations between $\epsilon_{e\mu}$ and C_b which contribute with opposite signs to $\sigma_{t\bar{t}}$) were thus taken into account. The total uncertainties on $\sigma_{t\bar{t}}$ and ϵ_b were calculated by adding the effects of all the individual systematic components in quadrature, assuming them to be independent. The sources of systematic uncertainty are discussed in more detail below.

$t\bar{t}$ modelling: Uncertainties on $\epsilon_{e\mu}$ and C_b due to the simulation of $t\bar{t}$ events were assessed as the differences between the predictions of the baseline Powheg+Pythia sample and one generated using MC@NLO+Herwig, thus varying both the hard-scattering event generator and the fragmentation and hadronisation model. The MC@NLO+Herwig sample gave a larger value of $\epsilon_{e\mu}$ but a smaller value of C_b, as shown in Table 3. Additional comparisons of Powheg+Pythia samples with the AUET2 rather than P2011C tune and with Powheg+Herwig, *i.e.* changing only the fragmentation/hadronisation model, gave smaller uncertainties. The Alpgen+Herwig sample gave a value of $\epsilon_{e\mu}$ 1.9 % higher than that of Powheg+Pythia, due largely to a more central predicted η distribution for the leptons. However, this sample uses a leading-order generator and PDFs, and gives an inferior description of the electron and muon η distributions (see Figures 2(c) and (e)), so was not

used to set the systematic uncertainty on $\epsilon_{e\mu}$. The ALPGEN+HERWIG prediction for C_b is close to that from POWHEG+PYTHIA, within the uncertainty set by the comparison to MC@NLO+HERWIG.

Initial/final state radiation: The estimates of $\epsilon_{e\mu}$ and C_b are sensitive to the amount of extra radiation in $t\bar{t}$ events through the lepton isolation and lepton-jet separation cuts, and changes in kinematic distributions. The effects were evaluated by taking half the difference between the predictions of two simulation samples generated with ACERMC+PYTHIA, with two tunes whose parameters span the variations compatible with ATLAS studies of additional jet activity in $t\bar{t}$ events [35]. The tune with more jet activity gives a smaller $\epsilon_{e\mu}$ and larger C_b. These variations also account for uncertainties on the modelling of the p_{T} of the $t\bar{t}$ system. The same generator combinations were used to assess the corresponding background uncertainties for Wt single top events.

Parton density functions: The uncertainties on $\epsilon_{e\mu}$ and the Wt single top background due to uncertainties on the proton PDFs were evaluated using the error sets of the CT10 [5], MSTW 2008 68 % CL NLO [4] and NNPDF 2.3 PDF [7] sets. The final uncertainty was calculated as half the envelope encompassing the predictions of all three PDF sets along with their associated uncertainties, following the PDF4LHC recommendations [3]. The value quoted in Table 3 also includes the much smaller effects of PDF variations on C_b, and the effects of correlations between the changes in ϵ_b and C_b.

QCD scale choices: The lepton p_{T} and η distributions, and hence $\epsilon_{e\mu}$, are sensitive to the choices of QCD renormalisation and factorisation scales. This effect was investigated using generator-level POWHEG+PYTHIA $t\bar{t}$ samples where the two scales were separately varied up and down by a factor of two from their default values of $Q^2 = {m_{\mathrm{top}}}^2 + p^2_{\mathrm{T,top}}$. The systematic uncertainty for each scale was taken as half the difference in $\epsilon_{e\mu}$ values between the samples with increased and decreased QCD scale, and the uncertainties for renormalisation and factorisation scales then added linearly to give a total scale uncertainty of 0.30 % on $\epsilon_{e\mu}$.

Single top modelling: Uncertainties related to Wt single top modelling were assessed by comparing the predictions from POWHEG+PYTHIA and MC@NLO+Herwig, and POWHEG interfaced to either PYTHIA or HERWIG, in all cases normalising the total production rate to the approximate NNLO cross-section prediction. The resulting uncertainties are 4.9 % and 23 % on the one and two b-tag background contributions. The background in the two b-tag sample is sensitive to the production of Wt with an additional b-jet, a NLO contribution to Wt which can interfere with the $t\bar{t}$ final state. The sensitivity to this interference was studied by comparing the predictions of POWHEG with the diagram removal and diagram subtraction schemes [36], giving additional single-top/$t\bar{t}$ interference uncertainties of 1.0 % and 20 % for the one and two b-tag samples. Production of single top quarks via the t- and s-channels gives rise to final states with only one prompt lepton, and is accounted for as part of the fake-lepton background.

Background cross-sections: The uncertainties on the Wt single top and diboson cross-sections were taken to be 6.8 % [33] and 5 % [34], based on the corresponding theoretical predictions.

Diboson modelling: Significant uncertainties exist in the modelling of diboson production with extra jets, in particular those with heavy flavour. The uncertainties in the backgrounds from dibosons with one or two additional b-tagged jets were assessed by comparing the baseline prediction from ALPGEN+HERWIG with that of SHERPA 1.41 [37]. The relative uncertainties are large (70 % and 200 % for one and two b-tagged events), but have a limited effect on the cross-section measurement due to the small absolute level of the diboson background.

Z+jets extrapolation: The uncertainties on the extrapolation of the Z+jets background from $Z \to \mu\mu$ to $Z \to \tau\tau$ events were assessed by comparing to the results from using $Z \to ee$ events, which have a different background composition.

Lepton-related uncertainties: The modelling of the electron and muon identification efficiencies, energy scales and resolutions were studied using $Z \to ee$ and $Z \to \mu\mu$ decays in data and simulation, using the techniques described in Refs. [25, 38]. Small corrections were applied to the simulation to better model the performance seen in data. These corrections have associated systematic uncertainties that were propagated to the cross-section measurement. The effect of the calorimeter and track isolation cuts applied to electrons and the track isolation cut applied to muons were also studied in detail using Z decays and found to be generally well-modelled, with systematic uncertainties again being propagated to the cross-section measurement.

Jet-related uncertainties: Although the efficiency to reconstruct and b-tag jets from $t\bar{t}$ events is extracted from the data, uncertainties in the jet energy scale, energy resolution and reconstruction efficiency affect the backgrounds estimated from simulation and the estimate of the tagging correlation C_b. They also have a small effect on $\epsilon_{e\mu}$ via the lepton-jet ΔR separation cuts. The jet energy scale was varied in simulation according to the uncertainties derived from simulation and an in-situ calibration measurement [30], using a model with 22 separate orthogonal uncertainty components which were then added in quadrature. The jet energy resolution has been found to be well-modelled in simulation, and remaining uncertainties were assessed by applying additional smearing [39], which reduces $\epsilon_{e\mu}$. The calorimeter jet reconstruction efficiency was measured in data using track-based jets, and is also well-described by the simulation; the impact of residual uncertainties was assessed by randomly discarding jets. The uncertainty associated with the jet vertex fraction requirement made on jets with $p_{\mathrm{T}} < 50\,\mathrm{GeV}$ was assessed by changing the cut value based on studies of $Z \to ee$+jets events [29].

b-tagging uncertainties: The efficiency for b-tagging b-jets from $t\bar{t}$ events was extracted from the data via equation (1), but simulation was used to predict the number of b-tagged jets and mistagged light quark, gluon and charm jets in the Wt single top and diboson backgrounds. The tagging correlation C_b is also slightly sensitive to the efficiencies for tagging both heavy- and light-flavour jets. The uncertainties in the simulation modelling of the b-tagging performance were assessed using studies of b-jets containing muons [32, 40], jets containing D^{*+} mesons [41] and inclusive jet events [42].

Pileup modelling: The simulated events were generated at a variety of instantaneous luminosities, spanning the range of conditions seen in the data. Events were reweighted based on μ, the average number of pileup events superimposed on each primary physics event, to reproduce the μ distribution seen in the data. The uncertainties were assessed by varying the correspondence between the simulated μ values and those estimated for data, reflecting uncertainties in the inelastic pp cross-section and the modelling of pileup events, with more simulated pileup leading to a reduction in $\epsilon_{e\mu}$.

Misidentified leptons: The uncertainties on the number of fake lepton events in the one and two b-tagged samples were derived from the statistical uncertainties on the numbers of same-sign lepton events, the systematic uncertainties on the opposite- to same-sign ratios R_j, and the uncertainties on the numbers of prompt same-sign events shown in Table 2, as discussed in detail in Section 4. The overall uncertainties on the numbers of misidentified leptons are 30 % and 52 % for the one and two b-tagged samples, dominated by the uncertainties on the ratios R_j.

Integrated luminosity: The uncertainty on the data integrated luminosity was evaluated to be 2.8 %, using techniques similar to those described in Ref. [43]. The relative effect on the cross-section measurement is slightly larger because the Wt single top and diboson backgrounds are evaluated from simulation, so are also sensitive to the assumed integrated luminosity.

LHC beam energy: The LHC beam energy during the 2012 pp run was recently calibrated to be 0.30 ± 0.66 % smaller than the nominal value of 4 TeV per beam, using the revolution frequency difference of protons and lead ions during p+Pb runs in early 2013 [44]. Since this calibration is compatible with the nominal $\sqrt{s}$ of 8 TeV, no correction was applied to the measured $\sigma_{t\bar{t}}$ value. However, an uncertainty of 1.7 %, corresponding to the expected change in $\sigma_{t\bar{t}}$ for an 0.66 % change in $\sqrt{s}$ [45] is quoted separately on the final result.

Top-quark mass: The simulation samples used in this analysis were generated with $m_{\text{top}} = 172.5$ GeV, but the acceptance for $t\bar{t}$ and Wt events, and the Wt background cross-section itself, depend on the assumed m_{top} value. Alternative samples generated with $m_{\text{top}} = 170$ and 175 GeV were used to quantify these effects. The acceptance and background effects partially cancel, and the final dependence of the result on the assumed m_{top} value was determined to be $\mathrm{d}\sigma_{t\bar{t}}/\mathrm{d}m_{\text{top}} = -0.26\,\%/\text{GeV}$. The result of the analysis is reported assuming a fixed top mass of 172.5 GeV, and the small dependence of the the cross-section on the assumed mass is not included as a systematic uncertainty.

The total systematic uncertainties on $\epsilon_{e\mu}$, C_b, and the fitted values of $\sigma_{t\bar{t}}$ and ϵ_b are shown in Table 3, and the systematic uncertainties on the individual background components are shown in Table 1. A more detailed breakdown is given in Table 4 in the Appendix. The dominant uncertainties on the cross-section result come from $t\bar{t}$ modelling, initial/final state radiation, PDFs and electron identification uncertainties. The uncertainties on the integrated luminosity and LHC beam energy also contribute significantly, and are quoted separately in the final result.

6 Additional correlation studies

The baseline Powheg+Pythia simulation sample predicts a small positive tagging correlation, $C_b = 1.007 \pm 0.002$, where the uncertainty is due to simulation statistics. Although the systematic uncertainty on C_b was set by the comparison with MC@NLO+Herwig (which gives $C_b = 1.001 \pm 0.002$), additional studies were carried out to probe the modelling of possible sources of correlation. One possible source is the production of additional $b\bar{b}$ or $c\bar{c}$ pairs in $t\bar{t}$ production, which tends to increase C_b, and the number of events with three or more b-tagged jets, which are not used in the measurement of $\sigma_{t\bar{t}}$. The ratio R_{32} of events with at least three b-tagged jets to events with at least two b-tagged jets was used to quantify this extra heavy-flavour production in data. It was measured to be $R_{32} = 2.7 \pm 0.2$ %, close to the Powheg+Pythia prediction of 2.4 ± 0.1 % (where the uncertainties in both cases are purely statistical), and well within the spread of R_{32} values seen in the alternative simulation samples.

Kinematic correlations between the two b-jets produced in the $t\bar{t}$ decay could also produce a positive tagging correlation, as the efficiency to reconstruct and tag b-jets is not uniform as a function of p_{T} and η. For example, $t\bar{t}$ pairs produced with high invariant mass tend to give rise to two back-to-back collimated top-quark decay systems where both b-jets have higher than average p_{T}, and longitudinal boosts of the $t\bar{t}$ system along the beamline give rise to η correlations between the two jets. These effects were probed by increasing the jet p_{T} cut in steps from the default of 25 GeV up to 75 GeV; above about 50 GeV, the simulation predicts strong positive correlations of up to *e.g.* $C_b \approx 1.2$ for a 75 GeV p_{T} cut. The cross-section fitted in data after taking these correlations into account remains stable across the full p_{T} range, suggesting that any such kinematic correlations are well-modelled by the simulation. The results were also found to be stable within the uncorrelated components of the statistical and systematic uncertainties

when tightening the jet and lepton η cuts, raising the lepton p_{T} cut up to 55 GeV and changing the b-tagging working point between efficiencies of 60 % and 80 %. No additional uncertainties were assigned as a result of these studies.

7 Summary and conclusion

The inclusive $t\bar{t}$ production cross-section has been measured using the full ATLAS 2012 pp collision data sample of 20.3 fb^{-1}at $\sqrt{s} = 8$ TeV, in the dilepton $t\bar{t} \to e\mu\nu\bar{\nu}b\bar{b}$ decay channel. The numbers of opposite-sign $e\mu$ events with one and two b-tagged jets were counted, allowing a simultaneous determination of the $t\bar{t}$ cross-section $\sigma_{t\bar{t}}$ and the probability to reconstruct and b-tag a jet from a $t\bar{t}$ decay. Assuming a top quark mass of $m_{\mathrm{top}} = 172.5$ GeV, the result is:

$$\sigma_{t\bar{t}} = 237.7 \pm 1.7\ (\mathrm{stat}) \pm 7.4\ (\mathrm{syst}) \pm 7.4\ (\mathrm{lumi}) \pm 4.0\ (\mathrm{beam\ energy})\ \mathrm{pb},$$

where the four uncertainties are due to data statistics, experimental and theoretical systematic effects, the integrated luminosity, and the LHC beam energy, giving a total relative uncertainty of 4.8 %. The dependence of the result on the assumed value of m_{top} is $\mathrm{d}\sigma_{t\bar{t}}/\mathrm{d}m_{\mathrm{top}} = -0.26\,\%/\mathrm{GeV}$, and the associated uncertainty is not included in the totals given above.

The measurement is consistent with and more precise than a previous result from ATLAS in the lepton+jets channel [46], and also with the theoretical prediction based on recent NNLO+NNLL calculations of $252.9^{+13.3}_{-14.5}$ pb at $m_{\mathrm{top}} = 172.5$ GeV.

References

[1] M. Cacciari et al., *Top-pair production at hadron colliders with next-to-next-to-leading logarithmic soft-gluon resummation*, Phys. Lett. B710 (2012) 612, arXiv:1111.5869;
P. Bärnreuther et al., *Percent Level Precision Physics at the Tevatron: First Genuine NNLO QCD Corrections to $q\bar{q} \to t\bar{t}$*, Phys. Rev. Lett. 109 (2012) 132001, arXiv:1204.5201;
M. Czakon and A. Mitov, *NNLO corrections to top-pair production at hadron colliders: the all-fermionic scattering channels*, JHEP 1212 (2012) 054, arXiv:1207.0236;
M. Czakon and A. Mitov, *NNLO corrections to top pair production at hadron colliders: the quark-gluon reaction*, JHEP 1301 (2013) 080, arXiv:1210.6832;
M. Czakon, P. Fiedler and A. Mitov, *The total top quark pair production cross-section at hadron colliders through $O(\alpha_S^4)$*, Phys. Rev. Lett. 110 (2013) 252004, arXiv:1303.6254.

[2] M. Czakon and A. Mitov, *Top++: a program for the calculation of the top-pair cross-section at hadron colliders*, arXiv:1112.5675.

[3] M. Botje et al., *The PDF4LHC Working Group Interim Recommendations*, arXiv:1101.0538.

[4] A.D. Martin et al., *Parton distributions for the LHC*, Eur. Phys. J. C63 (2009) 189, arXiv:0901.0002;
A.D Martin et al., *Uncertainties on α_s in global PDF analyses and implications for predicted hadronic cross sections*, Eur. Phys. J. C64 (2009) 653, arXiv:0905.3531.

[5] H.H. Lai et al., *New parton distributions for collider physics*, Phys. Rev. D82 (2010) 074024, arXiv:1007.2241.

[6] J. Gao et al., *The CT10 NNLO Global Analysis of QCD*, arXiv:1302.6246.

[7] R. D. Ball et al., *Parton distributions with LHC data*, Nucl. Phys. B867 (2013) 244, arXiv:1207.1303.

[8] M. Aliev et al., *HATHOR—Hadronic top and heavy quarks cross-section calculator*, Comp. Phys. Comm. A182 (2011) 1034, arXiv:1007:1327.

[9] ATLAS Collaboration, *The ATLAS Experiment at the CERN Large Hadron Collider*, JINST 3 (2008) S08003.

[10] ATLAS Collaboration, *The ATLAS Simulation Infrastructure*, Eur. Phys. J. C70 (2010) 823, arXiv:1005.4568.

[11] S. Agostinelli et al., *GEANT4: A simulation toolkit* , Nucl. Instr. Meth. A506 (2003) 250.

[12] ATLAS Collaboration, *The simulation principle and performance of the ATLAS fast calorimeter simulation FastCaloSim*, ATLAS-PHYS-PUB-2010-13, `http://cdsweb.cern.ch/record/1300517`.

[13] T. Sjöstrand, S. Mrenna, P. Skands, *A brief introduction to PYTHIA 8.1*, Comp. Phys. Comm. A178 (2008) 852, arXiv:0710.3820.

[14] P. Nason, *A new method for combining NLO QCD with shower Monte Carlo algorithms*, JHEP 0411 (2004) 040, arXiv:hep-ph/0409146;
S. Frixione, P. Nason, C. Oleari, *Matching NLO QCD computations with Parton Shower simulations: the POWHEG method*, JHEP 0711 (2007) 070, arXiv:0709.2092.

[15] S. Mrenna, T. Sjöstrand, P. Skands, *PYTHIA 6.4 physics and manual*, JHEP 05 (2006) 0265, arXiv:hep-ph/0603175.

[16] P.Z. Skands, *Tuning Monte Carlo Generators: The Perugia Tunes*, Phys. Rev. D82 (2010) 074018, arXiv:1005.3457.

[17] J. Erler and P. Langacker, *Electroweak model and constraints on new physics* in Particle Data Group, J. Beringer et al., *The Review of Particle Physics*, Phys. Rev. D86 (2012) 010001.

[18] S. Frixione and B. Webber, *Matching NLO QCD computations and parton shower simulations*, JHEP 06 (2002) 029, arXiv:hep-ph/0204244.

[19] G. Corcella et al., *HERWIG 6: An event generator for hadron emission reactions with interfering gluons (including supersymmetric processes)*, JHEP 101 (2011) 010, arXiv:hep-ph/0011363.

[20] J.M. Butterworth, J.R. Forshaw and M.H. Seymour, *Multiparton interactions in photoproduction at HERA*, Z. Phys. C72 (1996) 637, arXiv:hep-ph/9601371.

[21] ATLAS Collaboration, *New ATLAS event generator tunes to 2010 data*, ATLAS-PHYS-PUB-2011-008, `http://cdsweb.cern.ch/record/1345343`.

[22] M.L. Mangano et al., *ALPGEN, a generator for hard multiparton processes in hadronic collisions*, JHEP 0307 (2003) 001, arXiv:hep-ex/0206293.

[23] J. Pumplin et al., *New generation of parton distributions with uncertainties from global QCD analysis*, JHEP 07 (2002) 012, arXiv:hep-ph/0201195.

[24] B.P. Kersevan and E. Richter-Wąs, *The Monte Carlo event generator AcerMC version 2.0 with interfaces to PYTHIA 6.2 and HERWIG 6.5*, arXiv:hep-ph/0405247.

[25] ATLAS Collaboration, *Electron performance measurements with the ATLAS detector using the 2010 LHC proton-proton collision data*, Eur. Phys. J. C72 (2012) 1909, arXiv:1110.3174.

[26] K. Rethermann and B. Tweedie, *Efficient identification of boosted semileptonic top quarks at the LHC*, JHEP 1103 (2011) 059, arXiv:1007.2221

[27] M. Cacciari, G.P. Salam, *Dispelling the N^3 myth for the k_t jet-finder*, Phys. Lett. B641 (2006) 57, arXiv:hep-ph/0512210;
M. Cacciari, G.P. Salam and G. Soyez, *The anti-k_t jet clustering algorithm*, JHEP 04 (2008) 063, arXiv:0802.1189.

[28] ATLAS Collaboration, *Jet energy measurement with the ATLAS detector in proton-proton collisions at $\sqrt{s} = 7$ TeV*, Eur. Phys. J. C73 (2013) 2304, arXiv:1112.6426.

[29] ATLAS Collaboration, *Pileup subtraction and suppression for jets in ATLAS*, ATLAS-CONF-2013-083, `http://cdsweb.cern.ch/record/1570994`.

[30] ATLAS Collaboration, *Jet energy scale and its systematic uncertainty in proton-proton collisions at $\sqrt{s} = 7$ TeV with ATLAS 2011 data*, ATLAS-CONF-2013-004, `http://cdsweb.cern.ch/record/1509552`.

[31] ATLAS Collaboration, *Commissioning of the ATLAS high-performance b-tagging algorithms in the 7 TeV collision data*, ATLAS-CONF-2011-102, `http://cdsweb.cern.ch/record/1369219`.

[32] ATLAS Collaboration, *Measurement of the b-tag efficiency in a sample of jets containing muons with $5\,fb^{-1}$ of data from the ATLAS detector*, ATLAS-CONF-2012-043, `http://cdsweb.cern.ch/record/1435197`.

[33] N. Kidonakis, *Two-loop anomalous dimensions for single top quark associated production with a W^- or H^-*, Phys. Rev. D82 (2010) 054018, arXiv:1005.4451.

[34] J.M. Campbell and R.K. Ellis, *MCFM for the Tevatron and the LHC*, Nucl. Phys. Proc. Suppl. 205 (2010) 10, arXiv:1007.3492.

[35] ATLAS Collaboration, *Measurement of $t\bar{t}$ production with a veto on additional central jet activity in pp collisions at $\sqrt{s} = 7$ TeV using the ATLAS detector*, Eur. Phys. J. C72 (2013) 2043, arXiv:1203.5015.

[36] C. White, S. Frixione, E. Laenen and F. Maltoni, *Isolating Wt production at the LHC*, JHEP 11 (2009) 074, arXiv:0908.0631;
E. Re, *Single-top Wt-channel production matched with parton showers using the POWHEG method*, Eur. Phys. J. C71 (2011) 1547, arXiv:1009.2450.

[37] T. Gleisberg et al., *Event generation with Sherpa 1.1*, JHEP 02 (2009) 007, arXiv:0811.4622.

[38] ATLAS Collaboration, *Preliminary results on the muon reconstruction efficiency, momentum resolution and momentum scale in ATLAS 2012 pp collision data*, ATLAS-CONF-2013-088, `http://cdsweb.cern.ch/record/1580207`.

[39] ATLAS Collaboration, *Jet energy resolution in proton-proton collisions at $\sqrt{s} = 7$ TeV recorded in 2010 with the ATLAS detector*, Eur. Phys. J. C73 (2013) 2306, arXiv:1210.6210.

[40] ATLAS Collaboration, *b-tagging efficiency calibration using the System8 method*, ATLAS-CONF-2011-143, `http://cdsweb.cern.ch/record/1386703`.

[41] ATLAS Collaboration, *b-jet tagging calibration on c-jets containing D^{*+} mesons*, ATLAS-CONF-2012-039, http://cdsweb.cern.ch/record/1435193.

[42] ATLAS Collaboration, *Measurement of the Mistag Rate of b-tagging algorithms with 5 fb^{-1} of Data collected by the ATLAS Detector*, ATLAS-CONF-2012-040, http://cdsweb.cern.ch/record/1435194.

[43] ATLAS Collaboration, *Improved luminosity determination in pp collisions at $\sqrt{s}$ = 7 TeV using the ATLAS detector at the LHC*, Eur. Phys. J. C73 (2013) 2518, arXiv:1302.4393.

[44] J. Wenninger, *Energy Calibration of the LHC Beams at 4 TeV*, CERN-ATS-2013-40, http://cds.cern.ch/record/1546734.

[45] The numerical results were derived using the web interface at http://www.lpthe.jussieu.fr/~cacciari/ttbar/ .

[46] ATLAS Collaboration, *Measurement of the top quark pair production cross section in the single-lepton channel with ATLAS in proton-proton collisions at 8 TeV using kinematic fits with b-tagging*, ATLAS-CONF-2012-149, http://cdsweb.cern.ch/record/1493488.

Appendix

A more detailed breakdown of the systematic uncertainties is given in Table 4, for use in possible future combinations.

Uncertainty	$\Delta\epsilon_{e\mu}/\epsilon_{e\mu}$ (%)	$\Delta C_b/C_b$ (%)	$\Delta\sigma_{t\bar{t}}/\sigma_{t\bar{t}}$ (%)	$\Delta\sigma_{t\bar{t}}$ (pb)	$\Delta\epsilon_b/\epsilon_b$ (%)
Data statistics	-	-	0.72	1.7	0.57
$t\bar{t}$ modelling	0.91	-0.61	-1.52	-3.6	0.61
Initial/final state radiation	-0.76	0.26	1.23	2.9	0.37
Parton density functions	1.08	-	-1.09	-2.6	0.06
QCD scale choices	0.30	-	-0.30	-0.7	0.00
Single-top modelling	-	-	-0.38	-0.9	0.56
Single-top/$t\bar{t}$ interference	-	-	0.15	0.4	0.25
Single-top Wt cross-section	-	-	-0.70	-1.7	0.24
Diboson modelling	-	-	-0.42	-1.0	0.19
Diboson cross-sections	-	-	-0.03	-0.1	0.01
Z+jets extrapolation	-	-	-0.05	-0.1	0.02
Electron energy scale	0.43	0.00	-0.48	1.1	0.01
Electron energy resolution	-0.03	-0.01	0.04	0.1	0.02
Electron identification	1.20	0.00	-1.35	-3.2	0.05
Electron isolation	0.44	-	-0.44	-1.0	0.00
Muon momentum scale	0.01	-0.00	-0.03	-0.1	0.02
Muon momentum resolution	0.01	0.01	-0.04	-0.1	0.01
Muon identification	0.30	0.00	-0.34	-0.8	0.01
Muon isolation	0.40	-	-0.40	-1.0	0.00
Lepton trigger	0.15	0.00	-0.16	-0.4	0.01
Jet energy scale—model	0.22	0.03	0.23	0.5	0.06
Jet energy scale—statistics	0.05	0.02	0.08	0.2	0.04
Jet energy scale—detector	0.04	0.01	0.04	0.1	0.02
Jet energy scale—mixed	0.02	0.01	-0.04	-0.1	0.01
Jet energy scale—η intercalibration	-0.08	0.03	0.09	0.2	0.03
Jet energy scale—flavour response	-0.32	0.01	0.35	0.8	0.02
Jet energy scale—pileup	-0.23	0.03	0.20	0.5	0.06
Jet energy scale—high p_{T}	-0.00	-0.00	-0.01	-0.0	0.00
Jet energy scale—b-jets	0.00	0.01	-0.04	-0.1	0.03
Jet energy resolution	-0.44	0.04	0.59	1.4	0.08
Jet reconstruction efficiency	0.01	-0.01	-0.03	-0.1	0.01
Jet vertex fraction	0.01	0.01	-0.03	-0.1	0.00
b-tagging efficiency	-	0.11	-0.42	-1.0	0.07
b-tag mistagging	-	0.07	0.03	0.1	0.06
Pileup modelling	-0.30	0.05	0.28	0.7	0.05
Misidentified leptons	-	-	0.38	0.9	0.12
Total systematic	2.29	0.69	3.12	7.4	1.02
Integrated luminosity	-	-	-3.11	-7.4	0.11
LHC beam energy	-	-	-1.70	-4.0	0.00
Total uncertainty	2.29	0.69	4.77	11.3	1.17

Table 4: Detailed breakdown of the statistical, systematic and total uncertainties on the $t\bar{t}$ production cross-section $\sigma_{t\bar{t}}$ and the combined jet reconstruction and b-tagging efficiency ϵ_b. The systematic uncertainties on the $e\mu$ preselection efficiency $\epsilon_{e\mu}$ and the tagging correlation C_b are also shown, with relative signs given where relevant. The associated sign definitions are given in the text. The signs of the uncertainties on $\sigma_{t\bar{t}}$ are given using natural conventions, *e.g.* with a positive variation on an energy scale leading to an increase in estimated efficiency and a decrease in $\sigma_{t\bar{t}}$. For the jet energy scale uncertainty categories, each of which are composed of several components, a negative sign is given if all component variations are negative, and a positive sign otherwise.